Available online at www.sciencedirect.com
SCIENCE DIRECT®
Journal of Solid State Chemistry 177 (2004) 2477–2483
JOURNAL OF SOLID STATE CHEMISTRY
http://elsevier.com/locate/jssc

Solvothermal synthesis and crystal structure of Sb(III) and Sb(V) thioantimonates: $[Mn(en)_3]_2Sb_2S_5$ and $[Ni(en)_3(Hen)]SbS_4$

Ding-Xian Jia,[a] Yong Zhang,[a] Jie Dai,[a,b,*] Qin-Yu Zhu,[a] and Xiao-Mei Gu[a]

[a] Department of Chemistry and Chemical Engineering, Suzhou University, 1 Shizi St., Suzhou 215006, PR China
[b] State Key Laboratory of Coordination Chemistry, Nanjing University, Nanjing 210093 PR China

Received 7 January 2004; received in revised form 31 March 2004; accepted 6 April 2004

Abstract

Thioantimonate compounds of $[Mn(en)_3]_2Sb_2S_5$ (**1**) and $[Ni(en)_3(Hen)]SbS_4$ (**2**) (en = ethylenediamine) were prepared by reaction of transition metal chloride with Sb and S_8 powders under solvothermal conditions. Compound **1** consists of discrete $[Sb_2S_5]^{4-}$ anion, which is formed by corner-sharing SbS_3 trigonal pyramids. Compound **2** is composed of discrete tetrahedral $[SbS_4]^{3-}$ anion. The compounds **1** and **2** are charge compensated by $[M(en)_3]^{2+}$ cations, whereas in the crystal of **2** there is another counter ion of $[Hen]^+$. The results of the synthesis suggest that the temperature, the concentration and the existing states of the starting materials and so on are important for the structure and composition of the final products. In addition, the oxidation-state of antimony might be related to the molar ratio of the reactants. Excess amount of elemental S is beneficial to the higher oxidation-state of thioantimonate (V). Compound **1** decomposes from 150°C to 350°C, while compound **2** decomposes from 200°C to 350°C remaining Sb_2S_3 and NiSbS as residues.

Keywords: Solvothermal synthesis; Thioantimonate; Crystal structure; Thermoanalysis

1. Introduction

In recent years, a large number of thioantimonate-s(III) with organic cations [1–4], transition metal complex cations [5–18] and other cations [19,20] serving as counterions to $Sb_x^{III}S_y^{n-}$ anions, have been synthesized under hydro- or solvo-thermal conditions. The rich structural diversity of thioantimonates(III) results from variable coordination behaviors of Sb(III) atom caused by the stereochemically active lone pair [21]. Compared with the bewildering thioantimonates(III), on the other hand, the thioantimonates (V) are less explored and only a few examples were reported [22–25]. Furthermore, unlike $Sb_x^{III}S_y^{n-}$, the $[Sb^VS_4]^{3-}$ anions seldom interconnected to form polyanion and always exist as isolated tetrahedral $[Sb^VS_4]^{3-}$ anions [5] except that in some cases $[Sb^VS_4]^{3-}$ is bound to a $Sb_x^{III}S_y^{n-}$ polyanion[5] and metal cations [22,25].

For the thioantimonate(III) compounds, $Mn_2(en)_2Sb_2S_5$ [16] and $Mn(en)_3Sb_4S_7$ [17] (en = ethylenediamine) were synthesized from the same starting materials and under the same solvothermal conditions, but only with different reactant concentrations. In the former compound, $Sb_2S_5^{4-}$ unit and two octahedrally coordinated Mn(II) ions are covalently linked into infinite linear chains by Mn–S bonds and the chains are further connected to two-dimensional layer by weak Sb–S bonds. The latter compound contains isolated $Mn(en)_3^{2+}$ cations and infinite one-dimensional $(Sb_4S_7^{2-})_n$ anions. Besides the concentration of reactants, other factors, such as reactant molar ratio of starting materials, temperature and so on play influences on the structures of thioantimonate. Although it is difficult to discuss the rules of these influences, some efforts have been made. In general, a trend towards lower dimensionality of the $Sb_xS_y^{n-}$ framework with increasing size of the counterion is observed [17,26]. Recently, we had reported a discussion on the influences of the ion radii

*Corresponding author. Department of Chemistry and Chemical Engineering, Suzhou University, 1 Shizi St., Suzhou 215006, PR China. Fax: +86-512-65224783.
E-mail address: daijie@suda.edu.cn (J. Dai).

0022-4596/$ - see front matter © 2004 Elsevier Inc. All rights reserved.
doi:10.1016/j.jssc.2004.04.009

and the formation constants of $[M(en)_3]^{2+}$ on the structures of a series complexes with formula $[M(en)_3]_2Sn_2S_6$ (M = Mn, Co, Ni, Zn) [27].

To further elucidate the factors of influences on the structure and composition of thioantimonates, more extensive investigations are needed. From this point of view, we report here two thioantimonates of $[Mn(en)_3]_2Sb_2S_5$ (**1**) and $[Ni(en)_3(Hen)]SbS_4$ (**2**). The syntheses, structures and their relationships were discussed and the thermal behaviors were also concerned.

2. Experimental

2.1. Synthesis

2.1.1. Synthesis of $[Mn(en)_3]_2Sb_2S_5$ (1)

The reactant mixture of $MnCl_2 \cdot 4H_2O$ (0.5935 g, 3 mmol), Sb (0.3653 g, 3 mmol), S (0.2887 g, 9 mmol) and 8 mL en were loaded into a Teflon-lined stainless steel autoclave with inner volume of 15 mL. Then the sealed autoclave was heated to 180°C in 4 h and kept isothermal for 7 days. After cooled to ambient temperature, a pure phase of light-yellow chip crystals of **1** was obtained. The crystals suitable for X-ray analysis were filtered off, washed with ethanol and ether and stored under vacuum. The yield based on Sb is about 70%. The C, H, N analysis found: C 16.52%, H 5.64%, N 19.06%. Calc.: C 16.48%, H 5.53%, N 19.22%.

2.1.2. Synthesis of $[Ni(en)_3(Hen)]SbS_4$ (2)

The mixture of $NiCl_2 \cdot 6H_2O$ (0.7131 g, 3 mmol), Sb (0.3653 g, 3 mmol) and S (0.5771 g, 18 mmol) dissolved in 10 mL en was loaded into a Teflon-lined stainless steel autoclave. Then the sealed autoclave was heated to 180°C in 4 h and kept isothermal for 4 days. After cooled to ambient temperature, the products were filtered off, washed with ethanol and ether. The products consist of purple prism crystals of **2** and a small amount of orange-yellow chip crystals of **3**, a reported compound $[Ni(en)_3]Sb_2S_4$ [9]. Pure phase of **2** was obtained by careful collection of the purple crystals and the yield based on Sb is about 65%. The C, H, N analysis of **2** found: C 17.49%; H 6.12%; N 20.25%. Calc.: C 17.47%; H 6.05%; N 20.37%. A pure phase of **3** was obtained when the amount of elemental S decreased to Ni(II)/Sb/S molar ratio of 1:1:3. C, H, N analysis of **3** found: C 11.82%; H 4.01%; N 13.63%. Calc.: C 11.80%; H 3.96%; N 13.76%.

2.2. Physical measurements

Elemental analysis was carried out on an EA-1110 elemental analyzer. TG and DSC analysis was conducted on a TGA-DSC microanalyzer SDT 2960 and the samples were heated under a nitrogen stream of 100 mL min^{-1} with a heating rate of 5°C min^{-1}. Powder X-ray diffraction (XRD) patterns were collected on a D/MAX-3C diffractometer using graphite monochromatized Cu$K\alpha$ radiation ($\lambda = 1.5406$ Å) and operating at 40 kV and 30 mA.

2.3. Crystal structure determination

All measurements were carried out on the Rigaku Mercury CCD diffractometer at temperature of -80 ± 1°C using ω-scan methods with graphite monochromated Mo-$K\alpha$ radiation ($\lambda = 0.07107$ nm). The X-ray data of single crystals were collected to a maximum 2θ value of 55.0°. An empirical absorption correction was applied for all compounds and the data were corrected for Lorentz and polarization effects. The structures of **1** and **3** were solved by direct methods using the program SHELX97 [28] and the structure of **2** was solved by heavy-atom Patterson methods (PATTY) [29]. All the structures were expanded using Fourier techniques DIRDIF99 [30]. The non-hydrogen atoms were refined anisotropically. Hydrogen atoms were located in difference Fourier maps. The final cycle of full-matrix least-squares refinement on F^2 was based on observed reflections and variable parameters, and converged with unweighted and weighted agreement factors of $R1$ and $wR2$. A summary of the experimental details and selected results for compounds **1** and **2** is given in Table 1. Details of crystal data in CIF format are available via request from the Cambridge Crystallographic Data Centre (CCDC 228001–228003).

3. Results and discussion

3.1. Synthesis of the compounds

Bensch's group has synthesized two thioantimonates $Mn_2(en)_2Sb_2S_5$ (dark red, lath-like) [16] and $Mn(en)_3Sb_4S_7$ (orange, platelet) [17] under solvothermal conditions from Mn/Sb/S system (en–H_2O). As mentioned in Section 1, these two different compounds were synthesized under the same solvothermal conditions (molar ratio 2:2:5, temperature 125–130°C) and from the same starting materials except the reactant concentrations. In this work, the third compound of $[Mn(en)_3]_2Sb_2S_5$ (light-yellow, chip) was obtained form $MnCl_2$/Sb/S system (en) in 1:1:3 molar ratio, using manganese dichloride as starting material instead of Mn powder, at higher temperature of 180°C. The three compounds possess different structures and composition from each other, which suggests again that the structures of thioantimonate (III) compounds are variable and the reactant molar ratio, the existing states of the starting materials and especially the temperature are some

Table 1
Crystallographic data for $[Mn(en)_3]_2Sb_2S_5$ (**1**) and $[Ni(en)_3(Hen)]SbS_4$ (**2**)

Compound	**1**	**2**
Empirical formula	$[Mn(en)_3]_2Sb_2S_5$	$[Ni(en)_3(Hen)]SbS_4$
Formula weight ($g\,mol^{-1}$)	874.27	550.09
Dimensions (mm)	$0.39\times0.24\times0.20$	$0.70\times0.30\times0.30$
Color, habit	light-yellow, chip	purple, prism
Crystal system	Orthorhombic	Triclinic
Space group	$P2_12_12_1$ (No. 19)	$P\bar{1}$ (No. 2)
a (Å)	11.3491(8)	8.752(5)
b (Å)	16.2732(12)	9.393(6)
c (Å)	17.6055(11)	13.959(8)
α (°)	90	104.815(3)
β (°)	90	91.935(5)
γ (°)	90	110.307(6)
V (Å^3)	3251.5(4)	1031.0(10)
Z	4	2
T (K)	193	193
$D_{calc.}$ ($g\,cm^{-3}$)	1.786	1.772
μ (mm^{-1})	2.746	2.634
2θ (max) (°)	55.0	55.0
Measured reflections	32914	9855
Independent reflections	7438	4395
R_{int}	0.047	0.023
Observations	6849 ($I>2\sigma(I)$)	4238 ($I>3\sigma(I)$)
Variables	375	257
R_1	0.024 ($I>2\sigma(I)$)	0.022 ($I>3\sigma(I)$)
wR_2	0.044 ($I>2\sigma(I)$)	0.075 ($I>3\sigma(I)$)
Goodness of fit	0.778	1.02

important roles for the final products. In some systems, there are competitive reactions and the product is not homogeneous, such as $Mn_2(en)_2Sb_2S_5$ coexists with $Mn(en)_3Sb_4S_7$ [16] and **2** coexists with **3** (this work).

The oxidation-state of the antimony is clearly related to the molar ratio of reactants. Mixed phases of **2** and **3** were obtained with Ni(II)/Sb/S molar ratio of 1:1:6, whereas pure phase of thioantimonate (III) $[Ni(en)_3]Sb_2S_4$ (**3**) was obtained with Ni(II)/Sb/S molar ratio of 1:1:3. This result is in accordance with the facts reported in literatures that the Sb/S molar ratio varying from 1:2 to 1:3 results in thioantimonate (III) compounds, such as $[Ni(dien)_2]_3Sb_{12}S_{21}\cdot H_2O$ [13] (Sb/S = 1:2); $Mn_2(en)_2Sb_2S_5$ [16] and $Mn(en)_3Sb_4S_7$ [17] (Sb/S = 1:2.5); $[M(tren)]Sb_2S_4$ (M = Co, Ni) [7], $[Co(tren)_2]Sb_4S_8$ [8], $[Ni(en)_3]Sb_2S_4$ [9], $[Ni(dien)_2]_9Sb_{22}S_{42}\cdot0.5H_2O$ [10], $[Fe(dien)_2]Sb_6S_{10}\cdot0.5H_2O$ [12] and $[Fe(dien)_2]Fe_2Sb_4S_{10}$ [15] (Sb/S = 1:3). But when sulfur element increases to Sb/S molar ratio less than 1:3, the thioantimonate(V) compounds are produced under the same solvothermal conditions, such as $[Cr(en)_3]SbS_4$ [22] (Sb/S = 1:3.5), $[Mn(tren)(Htren)]SbS_4$ [25] (Sb/S = 1:4) and $[Ni(en)_3(Hen)]SbS_4$ (this work, Sb/S = 1:6). The excess amount of elemental S is beneficial to oxidize $Sb^{III}S_3^{3-}$ to $Sb^{V}S_4^{3-}$ in the presence of en, which is shown as follows:

$$Sb^{III}S_3^{3-}+S\xrightarrow{en}Sb^{V}S_4^{3-}. \quad (1)$$

It should be noted that the product of $[Ni(en)_3]Sb_2S_4$ (**3**) has been synthesized by Kanatzidis from a different reaction system of $NiCl_2/Na_3SbS_3/en$ (water solution) at 130°C and reported some years ago [9].

3.2. Crystal structure of $[Mn(en)_3]_2Sb_2S_5$ (1)

$[Mn(en)_3]_2Sb_2S_5$ crystallizes in the orthorhombic crystal system with space group $P2_12_12_1$ (No. 19). The crystal structure of **1** consists of discrete $[Sb_2S_5]^{4-}$ anions and $[Mn(en)_3]^{2+}$ cations. The $[Sb_2S_5]^{4-}$ anion is formed by two corner-sharing SbS_3 trigonal pyramids with Sb–S–Sb angle of 96.18(3)°. The terminal Sb–S_t bond distances varying from 2.3660(10) to 2.3880(10) Å are shorter than those of bridging Sb1–S3 and Sb2–S3 bonds which are 2.4950(10) Å (Table 2). The S–Sb–S angles ranging from 99.11(3) to 103.56(4)° deviate from the ideal value of 109.5°. The two SbS_3 trigonal pyramids are in *cis*-conformation, so $[Sb_2S_5]^{4-}$ anion shapes like a saddle (Fig. 1). The Sb–S distances and S–Sb–S angles are comparable with those of $Sr_2Sb_2S_5\cdot15H_2O$ [31], a reported thioantimonate having discrete $[Sb_2S_5]^{4-}$ anions. The average Sb–S distance (av. 2.414 Å) is much shorter than that of $Mn_2(en)_2Sb_2S_5$ (Sb–S av. 2.457 Å) [16]. In $Mn_2(en)_2Sb_2S_5$, the direct coordination of $[Sb_2S_5]^{4-}$ with $[Mn(en)]^{2+}$ and the weak interactions between Sb and S from different units elongate the Sb–S bond distances.

Both Mn^{2+} ions are 6-fold coordinated by three bichelate en ligands forming distorted octahedra

Table 2
Selected bond distances (Å) and angles (°) for **1** and **2**

$[Mn(en)_3]_2Sb_2S_5$ (**1**)			
Sb1–S1	2.3710(10)	Sb1–S2	2.3880(10)
Sb1–S3	2.4950(10)	Sb2–S3	2.4950(10)
Sb2–S4	2.3660(10)	Sb2–S5	2.3670(10)
Mn1–N1	2.306(3)	Mn1–N2	2.243(3)
Mn1–N3	2.274(3)	Mn1–N4	2.253(3)
Mn1–N5	2.270(3)	Mn1–N6	2.302(3)
Mn2–N7	2.278(3)	Mn2–N8	2.251(3)
Mn2–N9	2.283(3)	Mn2–N10	2.262(3)
Mn2–N11	2.264(3)	Mn2–N12	2.293(3)
S1–Sb1–S2	103.40(3)	S1–Sb1–S3	99.11(3)
S2–Sb1–S3	100.59(3)	S4–Sb2–S5	103.56(4)
S3–Sb2–S4	100.96(3)	S3–Sb2–S5	101.87(3)
Sb1–S3–Sb2	96.18(3)		
$[Ni(en)_3(Hen)]SbS_4$ (**2**)			
Sb1–S1	2.3460(10)	Sb1–S2	2.3380(10)
Sb1–S3	2.3350(10)	Sb1–S4	2.3420(10)
Ni–N1	2.132(2)	Ni–N2	2.132(2)
Ni–N3	2.119(2)	Ni–N4	2.106(2)
Ni–N5	2.126(2)	Ni–N6	2.124(2)
S1–Sb1–S2	108.96(2)	S1–Sb1–S3	112.46(2)
S2–Sb1–S3	106.68(3)	S1–Sb1–S4	111.17(4)
S2–Sb1–S4	106.12(3)	S3–Sb1–S4	111.13(5)

manifested by the octahedral axial N–Mn–N_{trans} angles varying from 163.72(12)° to 173.23(11)°. The Mn–N distances being 2.243(3)–2.306(3) Å (Table 2) are typical for Mn^{2+} cation in an octahedral coordination environment of amine donor atoms [32,33]. The two $[Mn(en)_3]^{2+}$ cations show different conformations of $\Lambda(\delta\delta\lambda)$ and $\Delta(\lambda\lambda\lambda)$, which are shown in Fig. 2.

In the unit cell of **1**, four $[Sb_2S_5]^{4-}$ anions are located at cell-faces and two lie within the unit cell (Fig. 3). Between anions and cations, there are many N–H···S intermolecular hydrogen bonds with H···S distances ranging from 2.579(2) to 2.813(4) Å and N–H···S angles ranging from 141.17° to 170.12° resulting in a three-dimensional arrangement of the anions and cations. Every $[Sb_2S_5]^{4-}$ anion has interactions to eight different $[Mn(en)_3]^{2+}$cations by N–H···S hydrogen bonds.

3.3. Crystal structure of $[Ni(en)_3(Hen)]SbS_4$ (**2**)

The crystal structure of compound **2** consists of discrete tetrahedral $[SbS_4]^{3-}$ anion with $[Ni(en)_3]^{2+}$ and protonated $[Hen]^{+}$ cations serving as charge compensating ions (Fig. 4a). The Sb–S bond distances varying from 2.3350(10) to 2.3460(10) Å and S–Sb–S angles ranging from 106.12(3)° to 112.46(2)° (Table 2) are in agreement with compounds containing tetrahedral $[SbS_4]^{3-}$ anion [22,25]. The Ni^{2+} ion is coordinated by six N atoms from three en ligands with octahedral axial N–Ni–N_{trans} angles varying from 173.44(8)° to 173.76(8)(1)°. The conformation of $[Ni(en)_3]^{2+}$ octahedron is $\Lambda(\delta\delta\lambda)$ (Fig. 4a). The Ni–N distances of **2** vary from 2.106(2) to 2.132(2) Å. The protonated en molecule shows *cis* conformation (Fig. 4a) with torsion angle N(7)–C(7)–C(8)–N(8) of 62.5(2)°.

Unlike $[Cr(en)_3]SbS_4$ [22], which was also prepared in en under solvothermal conditions, the structure of **2** contains both coordinated and protonated amines. This difference may result from the valence of transition metal ions, because in **2**, the SbS_4^{3-} anion needs additional one protonated $[Hen]^{+}$ cation to compensate its negative charge. For the same reason, [Mn(tren)(Htren)]SbS_4 [25] also contains a protonated amine ion.

Both $[Ni(en)_3]^{2+}$ and $[Hen]^{+}$ cations interact with $[SbS_4]^{3-}$ anion via N–H···S hydrogen bonding (Fig. 4b). The H···S distances between $[SbS_4]^{3-}$ and $[Ni(en)_3]^{2+}$ (varying from 2.539(2) to 2.89(4) Å) are slightly longer than those between $[SbS_4]^{3-}$ and $[Hen]^{+}$ (varying from

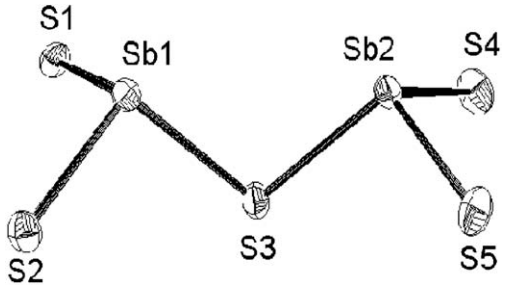

Fig. 1. The ORTEP view of the $[Sb_2S_5]^{4-}$ anion structure in compound **1** with labeling (50% probability ellipsoids).

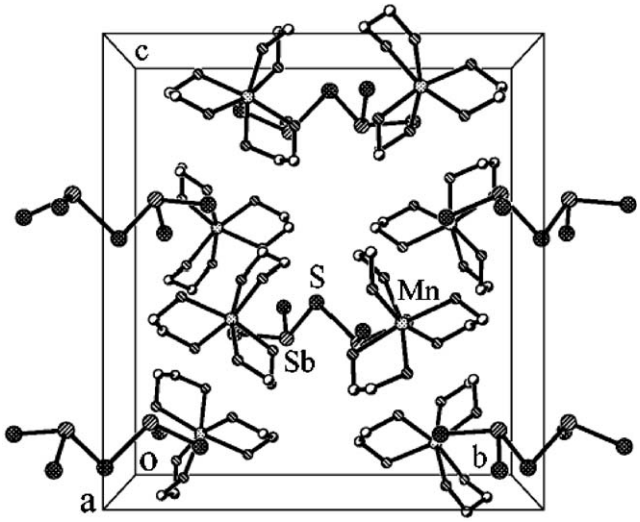

Fig. 3. The unit cell packing of the $[Sb_2S_5]^{4-}$ anions and the $[Mn(en)_3]^{2+}$ cations in **1**. Hydrogen atoms are omitted for clarity.

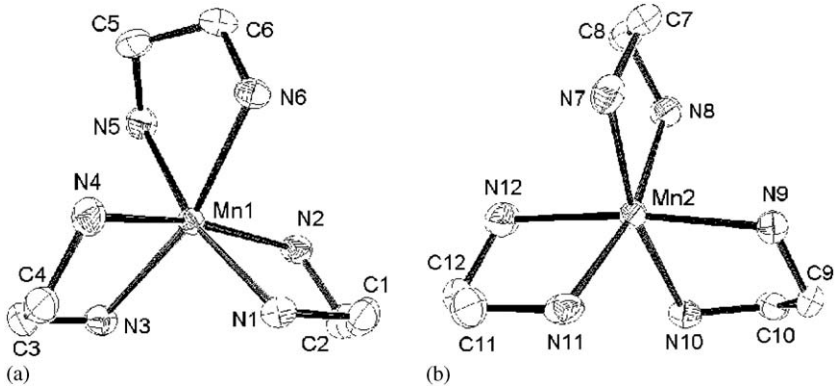

Fig. 2. The ORTEP views of the $[Mn(en)_3]^{2+}$ cation structures in **1**, showing different conformations of $\Lambda(\delta\delta\lambda)$ (a) and $\Delta(\lambda\lambda\lambda)$ (b) with labeling (50% probability ellipsoids). Hydrogen atoms are omitted for clarity.

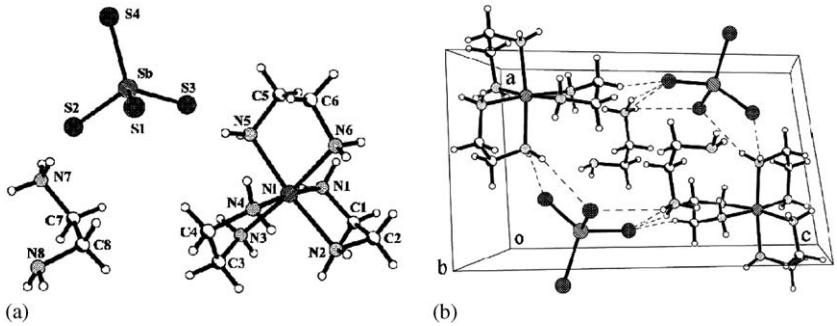

Fig. 4. Views of (a) the structure of $[Ni(en)_3(Hen)]SbS_4$ (**2**) with labeling and (b) the crystal packing (view along *b*-axis) of **2** with hydrogen bonds shown in dash lines (50% probability ellipsoids).

Table 3
Selected H···S distances (Å) and N–H···S angles (°) in $[Ni(en)_3(Hen)]SbS_4$ (**2**)

N–H	S	H···S	N···S	N–H···S
N(3)–H(9)	S(1)	2.838(3)	3.662	152.7(2)
N(5)–H(17)	S(1)	2.790(2)	3.614	155.6(2)
N(7)–H(26)	S(1)	2.74(5)	3.513(3)	147.7(43)
N(8)–H(29)	S(1)	2.780(2)	3.586(3)	145.7(2)
N(4)–H(11)	S(2)	2.539(2)	3.387(2)	160.1(2)
N(7)–H(27)	S(2)	2.403(2)	3.174(2)	158.9(2)
N(1)–H(1)	S(3)	2.741(2)	3.572(3)	156.5(2)
N(2)–H(3)	S(3)	2.89(4)	3.655	147.7(23)
N(5)–H(18)	S(3)	2.578(2)	3.423(3)	156.0(2)
N(6)–H(20)	S(3)	2.672(2)	3.473(2)	149.2(2)
N(1)–H(2)	S(4)	2.820(2)	3.628	151.4(2)
N(6)–H(19)	S(4)	2.83(3)	3.634	149.7(22)
N(7)–H(25)	S(4)	2.54(4)	3.409(3)	164.2(24)

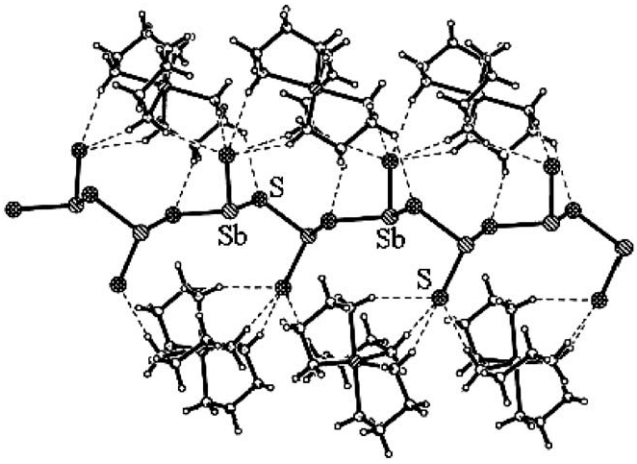

Fig. 5. The view of the infinite $[SbS_2]^-$ chain and complex cations in compound **3** with hydrogen bonds shown in dash lines.

2.403(2) to 2.780(2) Å) (Table 3). The shortest distance of N–H···S among all hydrogen bonds is 3.174 Å (N(7)–H(27)···S(2), between $[SbS_4]^{3-}$ and $[Hen]^+$).

The structure of the co-crystallized compound $[Ni(en)_3]Sb_2S_4$ (**3**) is essential identical to the former reported one [9], although they were prepared from different starting materials and at different temperature. Therefore the structure of **3** is not described here again except that the en ligands in present determination are completely ordered, but they are disordered in the reported data [9]. Because the temperature of CCD measurement was at −80°C, the N–H···S interactions between anionic chain and complex cations are increased, which are able to anchor N atoms at certain positions. Fig. 5 shows the N–H···S hydrogen bonds between the anion chain and complex cations.

3.4. Thermal analyses

The thermal behaviors of compounds **1** and **2** were measured with TG-DSC method under nitrogen stream. The results are shown in Fig. 6. It can be assumed that the mass loss about 4.3% bellow 100°C in the first stage of compound **1** is due to desorption of physisorption water. Compound **1** removes organic ligands roughly in two steps with corresponding mass loss of 21.4% and 18.8%, respectively. The total mass loss of 40.2% is in accordance with theoretical value of complete mass losses of six en ligands (calc. 41.2% for 6 en). The two decomposition steps are accompanied by two endothermic peaks at temperature (T_p) 152.9°C and 195.7°C, respectively, on DSC curve (Fig. 6a).

The thermal decomposition behavior of compound **2** is in a different pattern (Fig. 6b). In the first step, compound **2** decomposes with a mass loss of 11.0% which corresponds with removing one en ligand (calc. 10.9% for 1 en). In the following two steps, **2** loses three en ligands, and then 0.5 molecular H_2S with corresponding mass loss of 36.6% altogether (calc. 32.8% for 3 en + 3.1% for $0.5H_2S$) (Fig. 6b). The total mass loss of 46.6% is in good agreement with theoretical mass loss of 46.8%. The three mass loss steps concur with three endothermic signals at 200.1°C, 234.5°C and 265.8°C, respectively, on DSC curve (Fig. 6b). The phase of residue of **2** at 400°C was checked by X-ray diffraction method and the result is shown in Fig. 7. All the XRD peaks can be indexed to orthorhombic antimony (III) sulfide (Sb_2S_3, JCPDS No. 6-0474) and Ullmannite of

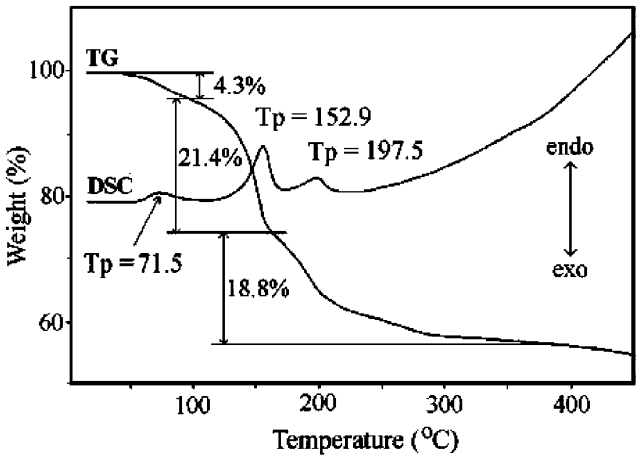

(a)

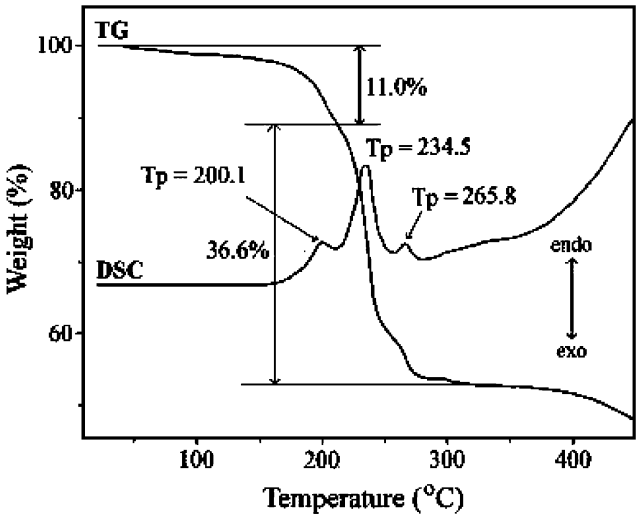

(b)

Fig. 6. TG-DSC curves of the compounds **1** (a) and **2** (b).

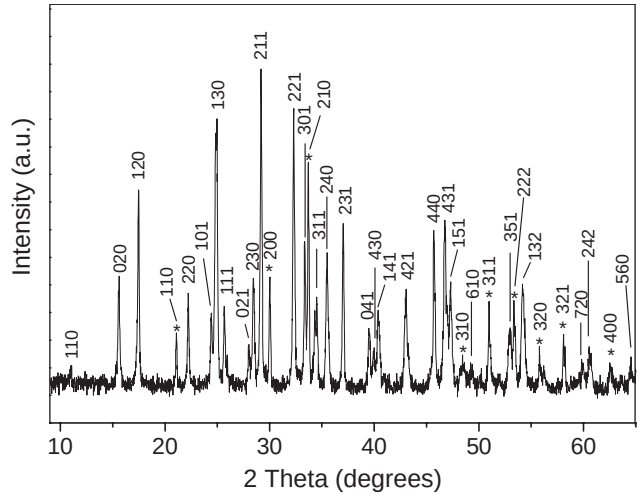

Fig. 7. The powder XRD pattern of thermoanalytical residues of **2** at 400°C. The peaks are indexed to Sb_2S_3 (no mark) and Ullmannite NiSbS (marked with *).

cubic nickel antimony sulfide (NiSbS, JCPDS No. 41-1472), respectively. So at 400°C, **2** decomposes to a mixture of Sb_2S_3 and NiSbS.

4. Conclusions

Thioantimonates $[Mn(en)_3]_2Sb_2S_5$ (**1**) and $[Ni(en)_3(Hen)]SbS_4$ (**2**) were obtained from MCl_2 (M = Mn, Ni)/Sb/S/en synthetic system under solvothermal conditions. In addition to the concentration, the existing states of the starting materials, the temperature and so on, it is found that the oxidation-state of the antimony is also related to the molar ratio of reactants. The molar ratio of MCl_2/Sb/S/ = 1:1:3 gives thioantimonates(III), whereas the ratio of 1:1:6 yields thioantimonate(V) in condition of this work. The excess amount of elemental S is beneficial to oxidize $Sb^{III}S_3^{3-}$ to $Sb^{V}S_4^{3-}$.

Acknowledgments

This work was supported by the National Natural Science Foundation (20071024, 20371033), PR China. The authors are also grateful to the Key Laboratory of Organic Synthesis of Jiangsu Province, Suzhou University, for financial support.

References

[1] L. Engelke, C. Näther, W. Bensch, Eur. J. Inorg. Chem. (2002) 2936.
[2] X. Wang, L. Liu, A.J. Jacobson, J. Solid State Chem. 155 (2000) 409.
[3] H. Rijnberk, C. Näther, W. Bensch, Monatsh. Chem. 131 (2000) 721.
[4] M. Schur, A. Gruhl, C. Näther, I. Jeß, W. Bensch, Z. Naturforsch. B 54 (1999) 1524.
[5] R. Stähler, B.-D. Mosel, H. Eckert, W. Bensch, Angew. Chem. Int. Ed. 41 (2002) 4487.
[6] H.-O. Stephan, M.G. Kanatzidis, J. Am. Chem. Soc. 118 (1996) 12226.
[7] R. Stähler, W. Bensch, Eur. J. Inorg. Chem. (2001) 3073.
[8] R. Stähler, W. Bensch, J. Chem. Soc. Dalton Trans. (2001) 2518.
[9] H.-O. Stephan, M.G. Kanatzidis, Inorg. Chem. 36 (1997) 6050.
[10] R. Stähler, W. Bensch, Z. Anorg. Allg. Chem. 628 (2002) 1657.
[11] W. Bensch, C. Näther, R. Stähler, J. Chem. Soc. Chem. Commun. (2001) 477.
[12] R. Stähler, C. Näther, W. Bensch, Eur. J. Inorg. Chem. (2001) 1835.
[13] R. Stähler, C. Näther, W. Bensch, J. Solid State Chem. 174 (2003) 264.
[14] M. Schaefer, C. Näther, W. Bensch, Solid State Sci. 5 (2003) 1135.
[15] R. Kiebach, W. Bensch, R.-D. Hoffmann, R. Pöttgen, Z. Anorg. Allg. Chem. 629 (2003) 532.
[16] M. Schur, W. Bensch, Z. Naturforsch. B 57 (2002) 1.
[17] W. Bensch, M. Schur, Z. Naturforsch. B 52 (1997) 405.
[18] M. Schur, C. Näther, W. Bensch, Z. Naturforsch. B 56 (2001) 79.
[19] A.V. Powell, S. Boissière, A.M. Chippindale, J. Chem. Soc. Dalton Trans. (2000) 4192.

[20] A.V. Powell, R. Paniagua, P. Vaqueiro, A.M. Chippindale, Chem. Mater. 14 (2002) 1220.
[21] M. Schur, W. Bensch, Z. Anorg. Allg. Chem. 624 (1998) 310.
[22] M. Schur, H. Rijnberk, C. Näther, W. Bensch, Polyhedron 18 (1998) 101.
[23] M. Schur, W. Bensch, Acta Crystallogr. C 56 (2000) 1107.
[24] R. Stähler, C. Näther, W. Bensch, Acta Crystallogr. C 57 (2001) 26.
[25] M. Schaefer, L. Engelke, W. Bensch, Z. Anorg. Allg. Chem. 629 (2003) 1912.
[26] M.G. Kanatzidis, Phosphorous, Sulfur Silicon 93–94 (1994) 159.
[27] D.-X. Jia, Y. Zhang, J. Dai, Q.-Y. Zhu, X.-M. Gu, Z. Anorg. Allg. Chem. 630 (2004) 313.
[28] G.M. Sheldrick, SHELX97, 1997.
[29] P.T. Beurskens, G. Admiraal, G. Beurskens, W.P. Bosman, S. Garcia-Granda, R.O. Gould, J.M.M. Smits, C. Smykalla, The DIRDIF program system, PATTY, Technical Report of the Crystallography Laboratory, University of Nijmegen, The Netherlands, 1992.
[30] P.T. Beurskens, G. Admiraal, G. Beurskens, W.P. Bosman, R. de Gelder, R. Israel, J.M.M. Smits, The DIRDIF-99 program system, DIRDIF99, 1999.
[31] G. Cordier, H. Schäfer, C. Schwidetzky, Rev. Chim. Miner. 22 (1985) 722.
[32] J. Li, Z. Chen, T.J. Emge, T. Yuen, D.M. Proserpio, Inorg. Chim. Acta 273 (1998) 310.
[33] F. Wendland, C. Näther, W. Bensch, Z. Anorg. Allg. Chem. 626 (2000) 456.